Fuel 288 (2021) 119585

Contents lists available at ScienceDirect

Fuel

journal homepage: www.elsevier.com/locate/fuel

Full Length Article

Measurements of the laminar burning velocities and NO concentrations in neat and blended ethanol and n-heptane flames

Marco Lubrano Lavadera *, Christian Brackmann, Gianluca Capriolo, Torsten Methling [1], Alexander A. Konnov

Division of Combustion Physics, Lund University, SE-22100 Lund, Sweden

ARTICLE INFO

Keywords:
Nitric oxide
Laminar burning velocity
LIF
Heat flux method
Ethanol
n-Heptane

ABSTRACT

Adiabatic laminar burning velocities and post-flame NO mole fractions for neat and blended ethanol and n-heptane premixed flames were experimentally determined using a heat flux burner and laser-induced fluorescence. The flames were stabilized at atmospheric pressure and at an initial temperature of 338 K, over equivalence ratios ranging from 0.6 to 1.5. These experiments are essential for the development, validation and optimization of chemical kinetic models, e.g. for the combustion of gasoline-ethanol fuel mixtures. It was observed that the addition of ethanol to n-heptane leads to an increase in laminar burning velocity that is not proportional to the ethanol content and to a decrease of NO formation. Such a NO reduction is due to the slightly lower flame temperatures of ethanol, which decrease the production of thermal-NO at $0.6 < \Phi < 1.2$, while under fuel-rich conditions this behavior is due to the lower concentrations of CH radicals, which decrease the production of prompt-NO. At $\Phi > 1.3$, the lower NO formation through the prompt mechanism in the ethanol flames is partially offset by a lower rate of NO consumption through the reburning mechanism. New experimental results were compared with predictions of the POLIMI detailed chemical kinetic mechanism. An excellent agreement between measurements and simulated results was observed for the laminar burning velocities over the equivalence ratio range investigated; however, discrepancies were found for the NO mole fractions, especially under rich conditions. Further numerical analyses were performed to identify the main causes of the observed differences. Differences found at close-to stoichiometric conditions were attributed to an uncertainty in the thermal-NO mechanism. In addition, disagreement under rich conditions could be explained by the relative importance of reactions in hydrogen cyanide consumption pathways.

1. Introduction

In recent years, the constantly fluctuating prices of crude oil, the depletion of its worldwide reserves and the more stringent governmental regulations on pollutant emissions, have stimulated a growing interest in the search for alternative fuels, with particular attention on biofuels. These renewable fuels contribute to a more sustainable energy supply and to the reduction of net CO_2 emissions from fossil sources. Among biofuels, ethanol is considered a promising candidate for gradually replacing conventional fuels in internal combustion engines, despite its low calorific value [1].

Ethanol as engine fuel is not a novel concept as it has been used since the end of 19th century and, nowadays, ethanol-based fuels are increasingly being used in "flex-fuel" spark-ignition (SI) engines because of their higher octane number compared with gasoline [2], or in compression ignition (CI) engines that use dual-injection strategies [3]. Combined with modern engine control systems, the use of ethanol leads to lower harmful exhaust emissions without deteriorating functional parameters of the engine [4–11]. Indeed, numerous experimental studies claimed that the use of ethanol-enriched fuels significantly reduces emissions of carbon monoxide, unburned hydrocarbons and soot compared to gasoline- and diesel-fueled engines, mainly due to the leaning effect caused by the oxygen content in ethanol; nevertheless, ethanol addition may adversely affect the production of harmful carbonyl species [12] and nitrogen oxides (NO_x) [7]; these concerns could become a significant barrier to ethanol market expansion.

Referring to NO_x, Masum et al. [9] published a review focused on the use of ethanol, either pure or blended with gasoline, in different SI

* Corresponding author at: Division of Combustion Physics, Lund University, P.O. Box 118, SE-221 00 Lund, Sweden.
E-mail address: marco.lubrano_lavadera@forbrf.lth.se (M. Lubrano Lavadera).
[1] German Aerospace Center (DLR), Institute of Combustion Technology, 70569 Stuttgart, Germany.

https://doi.org/10.1016/j.fuel.2020.119585
Received 7 May 2020; Received in revised form 22 September 2020; Accepted 23 October 2020
Available online 14 November 2020

engines, highlighting the inconsistencies among the various literature reports. In particular, NO_x emissions have been reported to increase [5,12–22], decrease [2,7,8,23–32] or being unaffected [33–39] when running on ethanol/gasoline at different blending ratios, if compared with the corresponding neat gasoline baseline. Similar inconsistencies were also observed in the case of CI engines [1,3,4,11,40–48]. Many investigations have been carried out to identify how the NO_x emission trends vary according to the ethanol content in the fuel mixture, but there are considerable inconsistencies even in the explanations, which make fundamental understanding incomplete.

For example, some authors [7,49] stated that, since temperature, fuel/air equivalence ratio, residence time and fuel composition are the main parameters affecting the formation of NO_x, there are no theoretical reasons for engine-out NO_x emission levels to increase with increasing ethanol content, and any increase in tailpipe emissions is a result of reduced effectiveness of the after-treatment system due to catalyst and engine control technologies. As a matter of fact, since the latent heat of vaporization of ethanol is higher than that of neat gasoline/diesel and the adiabatic flame temperature is lower due to the low calorific value, the in-cylinder peak temperature achieved during combustion, and thus thermal nitric oxide (NO), should be reduced [2]. On the other hand, ethanol has higher flame propagation speed compared to gasoline, which leads to a more rapid and complete combustion. This important factor may cause higher in-cylinder peak pressure and temperature, thus higher thermal-NO levels, depending on the ethanol content in the fuel blend and engine operating conditions [6]. Regarding CI engines running with ethanol–diesel blends, a similar opposing effect is given by the lower cetane number (thus increased ignition delay time) of ethanol in comparison with neat diesel fuel, which could lead to higher peak cylinder pressures and temperatures, depending on the amount of ethanol, injection timing and engine operating conditions [4,40,46,48]. Moreover, when ethanol is added to gasoline or diesel fuel, it increases the H/C atom ratio of the fuel and the availability of oxygen for the combustion process, leading to a coupled shift in temperature, fuel–air ratio and combustion duration and this, in turn, influences both thermal- and prompt-NO formation mechanisms in a rather complex way that also depends on the oxygen-sensing feedback control and catalyst [8,9,14,17,50]. Another reason for the observed inconsistencies is that the way in which this delicate balance impacts the increase/decrease of NO_x emissions also depends on vehicle type, engine speed and load, compression ratio, fueling method, conversion efficiency and internal exhaust gas recirculation [5,9,13,17,24,26]. Therefore, the published results are difficult to compare with each other.

Based on the literature studies, it follows that there is a lack of fundamental understanding pertaining to the effect of ethanol properties on NO_x formation trends in SI and CI engines. As a matter of fact, in all the cited papers the authors recommended further investigations as more stringent environmental standards will have to be met in the future. In this regard, from the studies carried out in complex full-engine systems, definitive inferences are rendered difficult by the numerous chemical and physical processes which occur simultaneously and are intimately coupled.

The description of the pertinent chemical reaction sequences leading to the formation and destruction of NO_x involves hundreds of chemical species and reactions whose rates depend on pressure, temperature and mixture composition. Then, to accurately assess each step of the combustion process and thus provide a reliable prediction of the interplay between the fuel structure and NO_x formation mechanisms, it is necessary to experimentally and computationally study chemical details under controlled conditions. In this context, adiabatic premixed laminar flames are very useful tools. They have the advantage of separating chemical kinetics from other processes that also occur in automotive engines, such as turbulence, fuel atomization and vaporization, heat losses, etc.

In this perspective, NO formation in premixed ethanol flames has been investigated in several works. Marques et al. [51] measured NO and CH concentrations in ethanol flames using Laser-Induced Fluorescence (LIF). Later on, Watson et al. [52,53] carried out similar fundamental premixed laminar flame experiments to investigate the relative differences in NO_x emissions between alkane and alcohol fuels. These studies restricted the attention to C_1-C_4 alcohols, including ethanol, and their respective alkane equivalents. Bohon et al. conducted probe [54] and LIF [55] measurements of NO concentrations to explore the non-thermal NO formation pathways in C_1-C_3 alcohol flames.

In the abovementioned works, lower NO formation was generally observed in alcohol flames in comparison to alkane equivalents, which was often attributed to reduction in thermal-NO due to lower adiabatic flame temperatures and reduction in prompt-NO due to lower CH radical concentrations. The interpretation of these results was assisted by detailed chemical kinetic models. In this context, premixed flames provide a stringent test for the validation of reaction mechanisms. However, although many comprehensive kinetic schemes are available in the literature, they exhibit great variability in the predictions of all NO formation routes, even for simple fuels like methane, due to remaining uncertainties in the pertinent chemistry, as shown in recent well-controlled laminar premixed flames experiments [56]. It is expected that the discrepancies will be higher if more complex fuels are considered, as the NO formation and consumption mechanisms are strongly coupled to the structure of the fuel molecule, especially under fuel-rich conditions [57].

Since commercial engine fuels are variable complex mixtures composed of hundreds hydrocarbons, fundamental experimental studies aimed at describing their combustion chemistry usually focus on surrogate fuels. n-Heptane is considered as a major component of surrogates for both gasoline and diesel fuels [58–64], i.e. a primary reference fuel. The chemical pathways of the n-heptane combustion contributing to NO_x formation have been investigated, albeit only in a few studies [65,66].

Based on these reasons, blends of ethanol and n-heptane are investigated in this study to obtain fundamental understanding relevant for the impact of ethanol addition on NO_x formation trends in internal combustion engines. In order to better understand the fundamental kinetic coupling during co-oxidation of n-heptane and ethanol mixtures, fundamental experimental data are clearly required. Such data, however, are very scarce. Experimental and computational results for turbulent flow reactor oxidation of an E85 surrogate containing ethanol/n-heptane mixtures have been presented in [67]. The authors demonstrated that at low temperatures ethanol oxidation is driven by n-heptane radical production. Dagaut and Togbé [68] performed experiments on the oxidation of ethanol/n-heptane blends (20/80 and 50/50) in a jet stirred reactor and proposed a kinetic model for representing the data. Van Lipzig et al. [69] were the first to acquire accurate data on laminar burning velocities (S_L) of ethanol, n-heptane and a mixture of them (50/50) using the heat flux method. Ignition delay times of n-heptane/ethanol blends at intermediate temperatures and high pressures were measured by Yang et al. [70] using shock tube experiments to investigate the influence of exhaust gas recirculation on auto-ignition behavior.

However, despite the aforementioned efforts, no fundamental combustion studies have been conducted so far to systematically determine the NO_x emissions of ethanol in comparison and in combination with n-heptane. Such fundamental understanding is of direct relevance to optimize the operating conditions of practical systems in order to meet increasingly stringent EU regulations. Additional research is therefore needed to develop and validate chemical kinetic mechanisms against reliable fundamental experimental data and to investigate possibilities of improving existing models.

This need is addressed in the present paper. Motivated by the above considerations, an experimental and computational study of premixed laminar flames of n-heptane, ethanol, and a mixture of them, is presented. The main objective of the present work is to acquire accurate experimental data of S_L and post-flame NO mole fraction profiles at atmospheric pressure, over a wide range of equivalence ratios (Φ). These

data are expected to be useful as targets for development, validation and optimization of detailed kinetic models. For this purpose, results are also compared with predictions from a comprehensive kinetic model to assess its performance and to identify areas for further improvement. Results are then analyzed to provide some insights about the effect of physicochemical properties of the fuel on dominant NO formation pathways.

2. Experimental and modeling details

Planar, adiabatic, premixed laminar flames were stabilized at atmospheric pressure on a perforated plate burner using the heat flux method. This flat-flame-based method [71] has been extensively used by many research groups for accurately measuring S_L of gaseous and liquid fuels since it creates stable steady flames that, at suitable conditions, can be considered one-dimensional, adiabatic and stretchless. A review of the method and its development, detailed descriptions of the experimental setup and data processing algorithms have been presented elsewhere [72], thus only the relevant elements are outlined here.

The experimental apparatus consists of a flat-flame burner composed of a 2 mm-thick brass plate attached to the burner head and perforated with 0.5 mm-diameter holes at a pitch of 0.7 mm. The burner plate has a nominal diameter of 3 cm and an effective perforation area of 6.69745 cm^2. It is surrounded by a heating jacket supplied with thermostatic water to keep its edge at a constant temperature of 368 K, while the temperature of the fresh gas mixture (T_g) is maintained at 338 K (±1 K) by a separate heating system in the plenum chamber, also supplied with water. The selection of such T_g allows to compare the present values of S_L with those reported by Van Lipzig et al. [69] to validate the experimental methodology. S_L was determined by varying the flow rate of the gas mixture until a uniform radial temperature distribution over the burner plate, recorded by eight T-type thermocouples (0.1 mm bare wire diameter) soldered in the burner plate, was achieved. For this condition, the net heat flux from/to the burner plate is zero and the velocity of the unburned gas is equal to the adiabatic laminar burning velocity.

A mixing panel provides controlled flows of the vaporized fuel and air to set the required equivalence ratio. The liquid fuel feeding system consists of a stainless steel cylinder pressurized with nitrogen to feed the fuel through a Coriolis liquid mass flow controller into a Controlled Evaporator Mixer (CEM), both made by Bronkhorst High-Tech. The CEM consists of a control valve, a mixing device and a heat exchanger, the temperature of which is controlled by a temperature controller that is part of the system. The required liquid flow rate is metered to the set-point value by a control valve that forms an integral part of the CEM system. The total uncertainty of the liquid flow rate is a sum of 0.5 g/h plus the stated flow repeatability of the liquid flow controller, which corresponds to 0.2% of the reading. Neat n-heptane and ethanol were used as delivered from Fisher Scientific in sealed bottles. The purity of n-heptane and ethanol was better than 99.5% and 99.97%, respectively. The amount of water that could be dissolved in the ethanol when refilling the fuel reservoir was estimated to be within its purity. Then, pure ethanol and n-heptane were mixed in one ratio (50 vol%). The liquid blend was prepared by mass using a Mettler Toledo AG-College balance with a readability of 0.1 g, stirred and left to settle for several hours. The physical properties relevant for the mixture preparation were taken from the literature and excess volumes were not considered. Since the excess volume at ambient temperature for the present mixture is about 0.4 cm^3/mol [73,74], the relative uncertainty of the blend concentration does not exceed 0.5%, which can be neglected compared to experimental uncertainties related to the mass flow controllers. Synthetic air was delivered by AGA (21% O_2, 1% relative uncertainty) and its required flow rates were metered by means of a Bronkhorst High-Tech digital thermal mass flow controller. Air was also used as a carrier gas to stimulate the evaporation process as a mixing component and to transport the vapor. The gas flow meter was calibrated before measurements using a MesaLabs Definer 220 positive displacement calibrator. The total uncertainty of the air flow rate is a sum of 1% stated accuracy of the calibrator plus the stated flow repeatability of the mass flow controller, which corresponds to 0.2% of the set operating conditions. In order to prevent fuel condensation throughout the fueling system, an electrically heated tube was used to connect the evaporator to the plenum chamber and its temperature was set equal to T_g.

A detailed analysis and quantification of experimental uncertainties was reported earlier [72] and the overall accuracy of S_L in the present measurements was estimated to be better than ± 1 cm/s. The equivalence ratio of the mixtures was varied from 0.6 to 1.5 with a maximum uncertainty of 0.02.

This experimental configuration coupled with LIF optical diagnostics provide a workable combination for testing nitrogen kinetics, since sensitive, quantitative, highly spatially resolved NO profiles can be non-intrusively measured under well-controlled conditions, and the one-dimensional configuration can be easily modeled. The setup previously described in detail in [56] for the LIF measurements of NO mole fraction was adopted in this work. Measurements were made by excitation of the $A^2\Sigma^+ \leftarrow X^2\Pi$ (0–0) vibronic band of NO using a combined Nd:YAG laser (Brilliant B, Quantel) and dye laser (Quantel TDL-90) system. The laser was tuned to the rather temperature-insensitive (in the 1500–2500 K range) $Q_2(26.5)$ NO transition at wavelength 225.5 nm in air. The ultraviolet beam was expanded using a telescope arranged with lenses of focal length f = -150 mm and f = +300 mm. A prism directed the expanded beam across the center of the burner surface, and an f = +500 mm spherical lens focused the beam above the burner center. This ultraviolet laser beam defined the measurement volume, which was imaged onto the slit of a spectrometer (Shamrock SR-500i-A-R, Andor). A longpass filter (LP02-224R-25, Semrock) was mounted in front of the slit for suppression of background such as flame luminescence and residual scattered laser light. The fluorescence signal in the (0–1) γ-band of the $A^2\Sigma^+ \rightarrow X^2\Pi$ NO transition at wavelength 236 nm was detected by a photomultiplier tube (model H9305-01, Hamamatsu) at the spectrometer exit, where an additional slit was mounted. The photomultiplier signal was recorded by a digital oscilloscope (Wavejet Touch 354, Lecroy) and fluorescence signal traces were collected by averaging over 128 laser shots.

The pulse energy used together with the beam focusing allowed to conduct measurements with a laser irradiance under saturated condition, which facilitates determination of quantitative NO mole fractions from the measured signal, with a detection limit around 1 ppm. To achieve highest possible degree of saturation in the present setup, measurements were made at average energies of 2–2.3 mJ/pulse. These signals were confirmed to be in the saturated regime in [56]. In addition to the measurements made with the laser tuned to the $Q_2(26.5)$ resonance, offline data were also recorded by tuning the laser to wavelength 225.38 nm in air, corresponding to a NO absorption minimum. This was done to remove possible LIF signal interference from O_2 and background signals, e.g. from stray light reflections or species chemiluminescence. The experimental LIF signal profile was determined by subtracting the background measured offline from the corresponding measurement made online. The peak value after background subtraction represents a saturated fluorescence signal that was post-processed for quantitative determinations.

In particular, the LIF signal was converted into NO mole fraction values using the calibration methodology proposed in [56], where the signal was measured for different levels of known NO seeding (below 100 ppm) in a fuel-lean (Φ = 0.5) 85% H_2-15% CO/air flame with negligible native NO formed. This calibration ensures no consumption of doped NO through the flame zone. The NO mole fraction (X_{NO}) can then be expressed according to Eq. (1):

$$X_{NO} = \left(\frac{\Delta X_{NO}}{\Delta F_{NO}}\right)_{cal} \frac{T_{flame}}{T_{cal}} \frac{f_{cal}}{f_{flame}} \frac{Q_{flame}}{Q_{cal}} F_{flame} \quad (1)$$

where subscripts *cal* and *flame* refers to the quantities above for the

calibration flame and the investigated flame, respectively. F is the LIF signal, the factor $(\Delta X_{NO}/\Delta F_{NO})_{cal}$ is the reciprocal of the linear fit of the calibration curve, f is the population of NO molecules in the probed energy level given by the Boltzmann distribution, T is the temperature, and Q the collisional quenching rate. The flames stabilized on the heat flux burner are assumed to burn under adiabatic conditions with respect to the burner. However, radiative heat losses – mainly from hot H_2O and CO_2 – are present in the post flame zone. Thus, temperatures above the burner were taken from the flame simulations, which included these radiative heat losses. Typically, for the investigated flames, the calculated temperatures at 10 mm above the burner are 30–60 K lower than the adiabatic temperatures, depending on the equivalence ratio. Population factors for these temperatures were obtained from the LIFBASE software [75]. Collisional quenching rates were calculated using product-zone mole fractions of N_2, O_2, H_2O, CO_2, H_2, and CO obtained from simulations together with collisional quenching cross-sections presented by Settersten et al. [76]. Details of simulations are provided below. Following the analysis described in [56], the experimental uncertainty of NO quantification using this procedure is within 8.7%.

The experimental conditions were simulated using the Chemkin-PRO software package with the steady, freely-propagating, isobaric, one-dimensional Premix laminar flame-speed code. Thermo-diffusion, multicomponent transport and downstream radiative heat losses were all considered in the simulations. In particular, heat losses were calculated with an optically-thin radiation model, which included Planck absorption coefficients of H_2O, CO, CO_2, CH_4, NO, and N_2O taken from [77] (soot is not formed in the investigated flames). Especially, computations have shown that radiative heat losses have significant influence on the predictions of thermal-NO [78], but negligible effects on S_L and on the internal structure of the reaction layer for the relatively fast flames studied here. However, this radiation effect becomes relevant for flames near the extinction limit [79]. Numerical solutions were obtained on increasingly finer grids until grid independence was achieved. To shift the simulated distances of the free flame to corresponding heights above the burner (HAB), the point of HAB = 0 mm was set to the point where the surface plate temperature was reached. The main goal of the kinetic modeling was to assess the feasibility of using current detailed thermochemical and transport models to simulate S_L and NO production for the investigated flames. It should be noted that, while numerous models for the prediction of NO_x are available in the literature (e.g. [80–83]), most of them were built to predict the combustion behavior of fuels over the C_1-C_3 range, and, therefore, they are not suitable for the present comparison where n-heptane and ethanol have been used. On the other hand, some detailed kinetic schemes that describe heavy hydrocarbons and alcohol combustion exist in the literature, but they have not been expanded to include NO_x modeling capability. Therefore, to the best of our knowledge, the POLIMI comprehensive model is the only one suitable for predicting NO_x in alcohols and alkanes with chain lengths above C_3. It is a hierarchical model that has been developed to predict the oxidation of a wide variety of fuels, from syngas up to jet- and diesel fuels and it also includes a sub-model for NO_x production and reburning [84]. The NO_x sub-set has been validated against experimental data obtained in jet stirred and plug flow reactors from 500 to 1450 K, for a wide range of fuels up to pressures of 20 bar and against laminar premixed methane flames. This model has already been successfully tested for flames of n-decane, p-xylene, and methylcyclohexane, either burning the neat fuel or blended with ethanol [85]. The complete mechanism includes 621 species and 27,369 reversible reactions with the associated thermochemical and transport data. For this study, we selected a sub-set of the detailed model (CRECK_2003_TPRF_HT_ALC_NOX) that only describes high-temperature oxidation (excluding soot formation), which includes 299 species involved in 8028 reversible reactions.

3. Results and discussion

In the present experiments, laminar burning velocities and NO mole fraction for ethanol, n-heptane and a mixture of them (50 liquid vol.%) burning in air were studied at atmospheric pressure. T_g was fixed at 338 K because at this temperature the saturation pressure of each investigated fuel is above its partial pressure over a wide range of Φ values. This allowed to cover equivalence ratios up to 1.5 avoiding fuel condensation. The experimental results on S_L and X_{NO} are tabulated in the Supplemental material, together with the associated experimental uncertainties.

A comparison of the present experimental data for S_L of ethanol (Fig. 1a), n-heptane (Fig. 1b) and their mixture (Fig. 1c) as a function of Φ with those obtained by van Lipzig et al. [69] and by Sileghem et al. [86,87] (corrected according to re-evaluation reported in [72]) is shown in Fig. 1; the three datasets have been obtained using the heat flux method.

The present results are in remarkably good agreement with existing literature data, thus such comparison confirms the consistency of the heat flux method experiments. However, it should be noted that at Φ = 0.6, 1.4 and 1.5 in the case of ethanol (Fig. 1a), as well as at Φ = 1.3 in the case of n-heptane (Fig. 1b), the agreement deteriorates with respect to the measurements by van Lipzig et al. as the experimental data do not overlap within the evaluated uncertainty. Regarding this, the authors stated that at the extreme sides of stoichiometry their experimental results could be affected by larger uncertainty. In addition, Sileghem et al. [86,87] noted that one of the reasons of the higher results obtained by van Lipzig et al. for rich mixtures can be upstream fuel condensation and thus leaner gas mixtures than expected. Indeed, in the present work, as well as in [86,87], the gas mixture was transported from the evaporator to the burner through a heated tube, while in the previous experiments [69] an unheated tube was employed for this purpose.

Another observation from Fig. 1 is that, while for ethanol/air flames (Fig. 1a) S_L are reported from Φ = 0.6 to Φ = 1.5, for the other investigated fuel/air mixtures (Fig. 1b, c) the Φ range shrinks to 0.7–1.3. This occurs on the lean side because of narrower flammability limits of n-heptane compared to ethanol, and on the rich side because of intrinsic flame instabilities manifested as cellularity. As such, these results were excluded from this comparison because they do not rigorously represent fundamental adiabatic S_L values. Cell formation in rich flames of heavy hydrocarbons is a typical limitation of the heat flux method, as discussed in [72]. However, such instabilities are expected to have negligible effects on X_{NO} measured in the post-flame zone, considering that, as observed during the experiments, cellularity is strongly sensitive to the inlet flow velocity, while X_{NO} is almost independent on it, at least around the adiabatic condition. It follows that ethanol flames appear to be more stable than n-heptane flames for the same Φ. This observation is consistent with the results reported by Holley et al. [88], who studied the extinction of premixed flames using mixtures of ethanol and n-heptane burning in air and found that ethanol flames are more resistant to extinction than n-heptane flames. They concluded that mixing ethanol with hydrocarbons to formulate fuels for SI engines could improve the overall engine performance due to improved stability.

In Fig. 2, the three sets of present S_L measurements are compared with each other and with numerical calculations to assess the predictive capability of the selected model for the investigated fuel mixtures. Model predictions are reported with lines, while the experimental data are reported with symbols. First of all, it can be observed that neat ethanol flames are characterized by higher S_L compared to n-heptane and ethanol/n-heptane flames and that S_L of the fuel blend are not weighted averages of values associated with the neat constituents. In this regard, it should be clarified that 50 vol% is the volumetric percentage of the liquid blend, but this composition results in a 71.5% ethanol/28.5% n-heptane gas phase mixture. Therefore, S_L of the fuel blend should be closer to ethanol values if the mixing rule was linear in the constituent concentrations. However, under lean conditions, S_L of the blend is very close to that of ethanol; then, with increasing the equivalence ratio, the blend is characterized by burning velocities that are very close to those of n-heptane. This trend is not completely

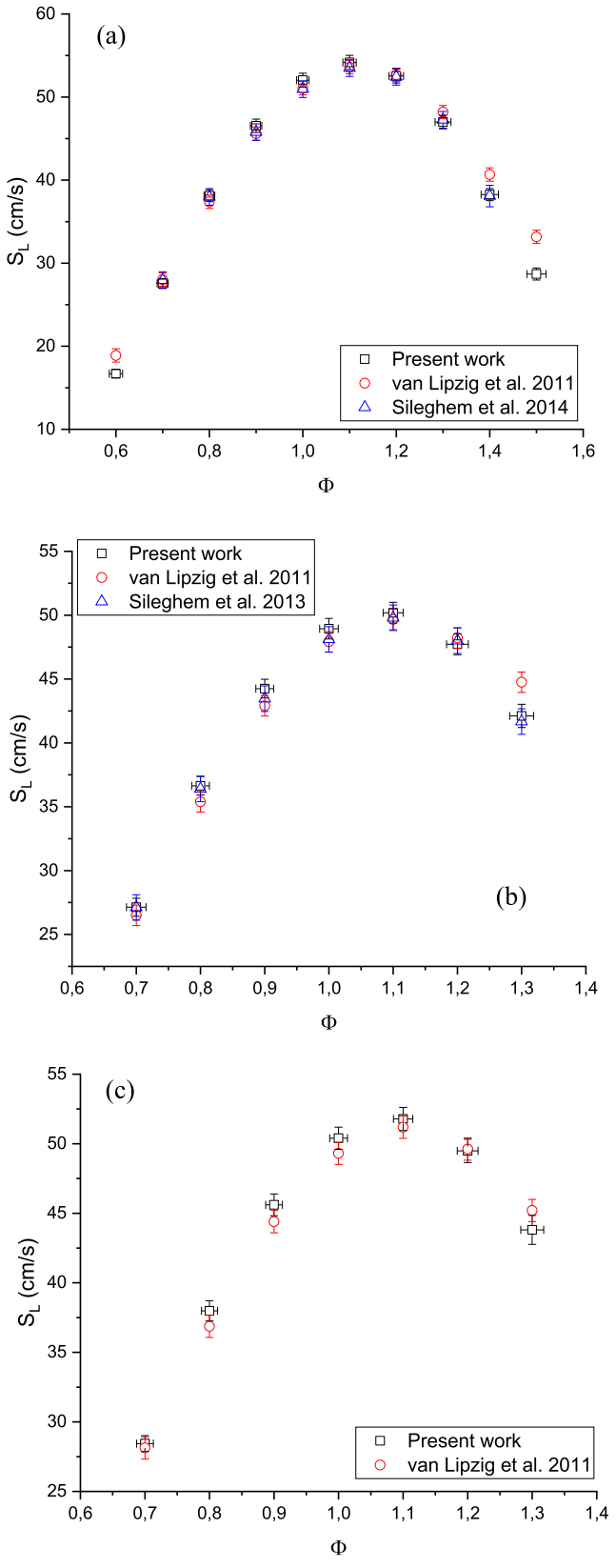

Fig. 1. Experimental S_L versus Φ at $T_g = 338$ K and $P = 1$ atm. Black squares: present work. Red circles: van Lipzig et al. [69]. Blue triangles: Sileghem et al. [86,87] (corrected according to the re-evaluation reported in [72]). (a) Ethanol/air mixtures. (b) n-heptane/air mixtures. (c) ethanol-n-heptane (50 vol %)/air mixtures. (For interpretation of the references to colour in this figure legend, the reader is referred to the web version of this article.)

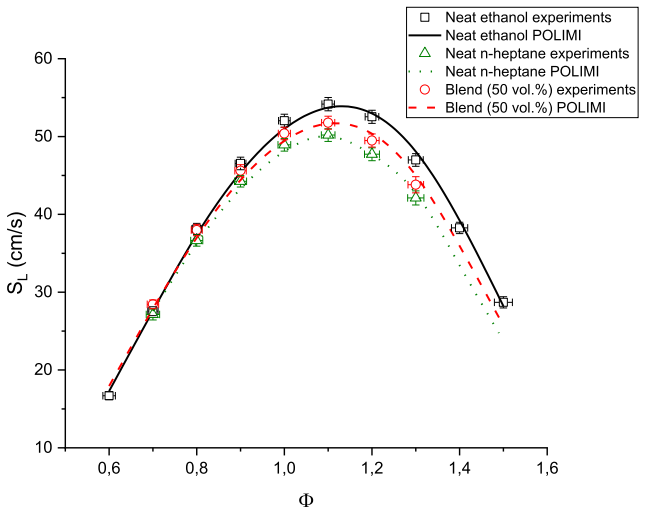

Fig. 2. Experimental (symbols) and simulated (lines) S_L versus Φ at $T_g = 338$ K and $P = 1$ atm. Black squares and solid line: Ethanol/air mixtures. Red circles and dashed line: ethanol-n-heptane (50 vol%)/air mixtures. Green triangles and dotted line: n-heptane/air mixtures. (For interpretation of the references to colour in this figure legend, the reader is referred to the web version of this article.)

unexpected considering that the variation of S_L as a function of the fuel composition do not follow the variation of the adiabatic flame temperature (ethanol has the lowest adiabatic flame temperature), suggesting that chemical kinetics, which is highly nonlinear with process parameters, has the dominant influence on the difference in burning velocity among the investigated fuels. In this regard, it was reported [89] that ethanol has a higher S_L compared to alkanes mainly due to the production of ethylene as primary intermediate species via the hydroxyethyl radical.

For the whole range of the fuels studied, there is an excellent agreement, both qualitatively and quantitatively, between measurements and predictions, as the model reproduces the measured S_L within the experimental uncertainty for all the equivalence ratios investigated. Such velocity predictions are very important for the identification of mixing rules for S_L as well as for accurate prediction of the residence times for NO formation through the thermal mechanism.

Results of NO LIF mole fraction measurements carried out in the post-flame zone are shown in Fig. 3 as a function of Φ together with the model predictions reported with lines. Each data point was averaged from 3 acquisitions and the experimental repeatability was excellent, with a variance well within the uncertainty given above. The effect of equivalence ratio on NO mole fraction was evaluated at a constant height above the burner surface (HAB = 10 mm) for consistency with previous measurements [56,82,90]. In the present tests, Φ ranged from very lean ($\Phi = 0.6$) to very rich ($\Phi = 1.5$) mixtures, with the exception of n-heptane/air flames, for which the condition $\Phi = 0.6$ was not possible to access due to stabilization problems. In Fig. 3 it can be seen that both Φ and fuel type are important parameters for NO formation. The experimental dependence of X_{NO} as a function of Φ is quite similar for the three investigated fuels. As Φ increases, X_{NO} rises until a peak is reached at $\Phi = 1$, then decreases until a plateau is reached at $\Phi > 1.2$, where the plateau trend is more marked for the ethanol containing fuels. The stoichiometric peak is mainly due to formation via the Zel'dovich thermal-NO mechanism, while in rich mixtures the plateau is due to the prompt-NO mechanism. However, even though qualitative similarities among the three fuels can be observed in the X_{NO} dependence on Φ, the impact of the fuel type is clearly reflected in different quantitative NO distributions.

In particular, Fig. 3 shows that ethanol/air flames produce lower levels of NO than the corresponding n-heptane/air flames under all the

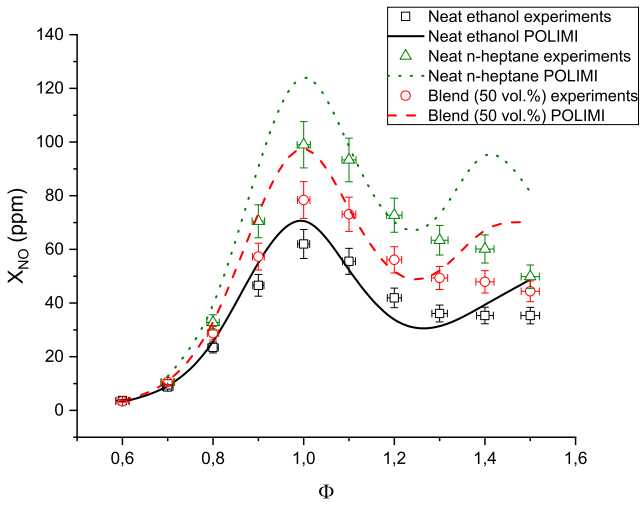

Fig. 3. Experimental (symbols) and simulated (lines) X_{NO} versus Φ at HAB = 10 mm, T_g = 338 K and P = 1 atm. Black squares and solid line: Ethanol/air mixtures. Red circles and dashed line: ethanol-n-heptane (50 vol%)/air mixtures. Green triangles and dotted line: n-heptane/air mixtures. (For interpretation of the references to colour in this figure legend, the reader is referred to the web version of this article.)

equivalence ratios investigated, with X_{NO} for the ethanol/n-heptane blend lying in between. The differences among NO produced from the three fuels also strongly depend on Φ. For example, the decrease of X_{NO} in the case of ethanol with respect to n-heptane varies from 17% at Φ = 0.7 to 43% at Φ = 1.3, while for the ethanol/n-heptane blend such decrease ranges from 0% at Φ = 0.7 to 23%, with the most prominent decrease observed at Φ = 1.2. Under stoichiometric conditions, the relative difference between X_{NO} produced from ethanol and the blend compared to n-heptane is 37% and 21% respectively. The trend observed from this comparison, even if related to premixed, atmospheric-pressure experiments, could at least qualitatively explain some of the inconsistencies found in the literature results presented for engine conditions [1–48], where the thermal-NO mechanism is recognized as the most relevant NO source. In particular, one observation is that X_{NO} is not very sensitive to the addition of ethanol under lean conditions. In this regard, it has to be noted that most of the literature results have been obtained using fuel blends with a lower concentration of ethanol with respect to the blend used in the present work. On the other hand, X_{NO} is very sensitive to the equivalence ratio, particularly at near-stoichiometric conditions. For example, X_{NO} measured at Φ = 1 for the blended fuel is higher than that measured in the case of pure n-heptane at Φ = 0.9.

Fig. 3 also presents the simulated results (lines) for NO in the post-flame zone using the POLIMI thermochemical model. Generally, the model is able to reproduce the key trends of the experiments at $\Phi < 1.2$ since experiments and simulations show similar variation in the magnitude of NO mole fraction as Φ is increased. However, while the trends of the experiments are preserved, the model tends to overpredict the peak X_{NO} by 9, 19 and 25 ppm for ethanol, ethanol/n-heptane and n-heptane, respectively. At higher Φ, large differences are also found in the qualitative behavior of the model compared with the experiments. In particular, the POLIMI model predicts an increase of X_{NO} at $\Phi > 1.2$ that is not observed experimentally. This is in agreement with previous observations reported in [52], where the POLIMI mechanism was used to predict burning velocities and NO concentrations in premixed flames of C_1-C_3 alkanes and alcohols, including ethanol. Consistent with the present work, the POLIMI, although a previous version, was found to predict the burning velocities well and overestimate the NO concentrations.

Notwithstanding, while an exact reproduction of the experimental X_{NO} is not achieved, the kinetic model tested in the present work is able to capture the observed effect of fuel type in altering X_{NO}. Hence, the detailed chemical kinetic model can help us to investigate the reasons contributing to the observed trends as a function of fuel nature.

Fig. 4 shows the variation of the flame temperature calculated at HAB = 10 mm as a function of the equivalence ratio for the three investigated fuels. By comparing Figs. 3 and 4 it is possible to observe that the variations of X_{NO} as a function of Φ (Fig. 3) for the three fuels appear to closely follow the variations of the flame temperature (Fig. 4), at least for $0.6 < \Phi < 1.2$. This observation suggests that in this equivalence ratio range the coupling between fuel and NO_x kinetics has a minor effect on X_{NO} and the dominant influence is given by the flame temperature, which confirms the thermal-NO as the predominant mechanism under lean and near-stoichiometric flame conditions. For ethanol flames, the lower flame temperature is not only due to the lower calorific value but also to the higher heat capacity due to the presence of more triatomic molecules in the combustion products, at a fixed equivalence ratio.

As seen in Fig. 3, for the near-stoichiometric flames (Φ = 0.9–1), i.e. where the thermal-NO pathway dominates due to very high temperatures, the reaction mechanism overpredicts the NO formation rate. This discrepancy becomes less pronounced, however, when moving from n-heptane to ethanol, i.e., as the flame temperature is decreased. Nevertheless, it is not easy to discern if the model weakness only lies in the thermal-NO sub-model or if it is also linked to the fuel-oxidation chemistry. To understand the reasons for the observed discrepancy and the improvements that need to be made, a local sensitivity analysis was performed for the three fuels at Φ = 1. The Chemkin-PRO software was used for calculation of normalized sensitivity coefficients provided in Fig. 5.

As already mentioned, under stoichiometric conditions the thermal-NO pathway has the highest impact on the overall NO formation. This can also be clearly seen in Fig. 5, where the reaction $N_2 + O = NO + N$ (R1) shows the highest sensitivity coefficients, with the reactions related to other NO formation mechanisms having lower impact. Furthermore, formation of NO through the thermal mechanism is also dependent on the O/H radical pool, which is typically controlled by the fuel oxidation chemistry. As a matter of fact, the chain branching reaction $H + O_2 = OH + O$ (R2) also shows high sensitivity coefficients. However, a very good agreement between the measured and predicted S_L (see Fig. 2) implies that both residence time and fuel oxidation chemistry are well reproduced in the simulations. This means that the issues in modeling

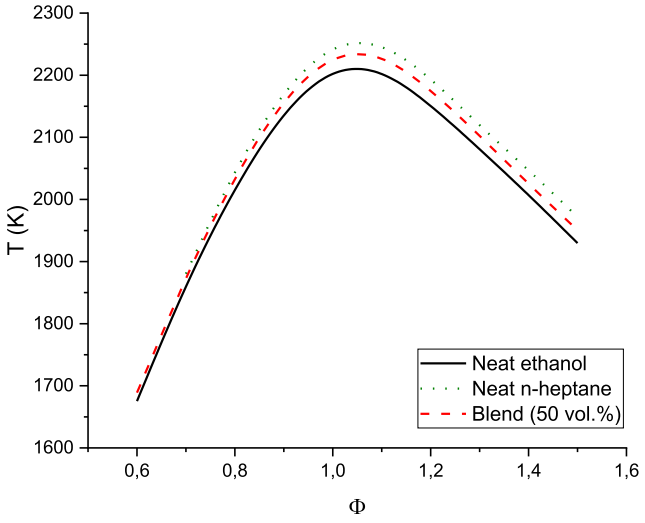

Fig. 4. Calculated flame temperature (T) versus Φ at HAB = 10 mm, T_g = 338 K and P = 1 atm. Black solid line: Ethanol/air mixtures. Red dashed line: ethanol-n-heptane (50 vol%)/air mixtures. Green dotted line: n-heptane/air mixtures. (For interpretation of the references to colour in this figure legend, the reader is referred to the web version of this article.)

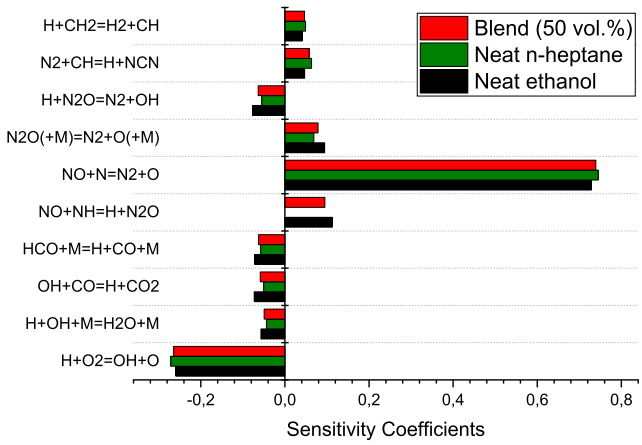

Fig. 5. Normalized NO sensitivity coefficients calculated at $\Phi = 1$, HAB = 10 mm, $T_g = 338$ K and $P = 1$ atm for ethanol/air mixtures (black bars), ethanol-n-heptane (50 vol%)/air mixtures (red bars) and n-heptane/air mixtures (green bars). (For interpretation of the references to colour in this figure legend, the reader is referred to the web version of this article.)

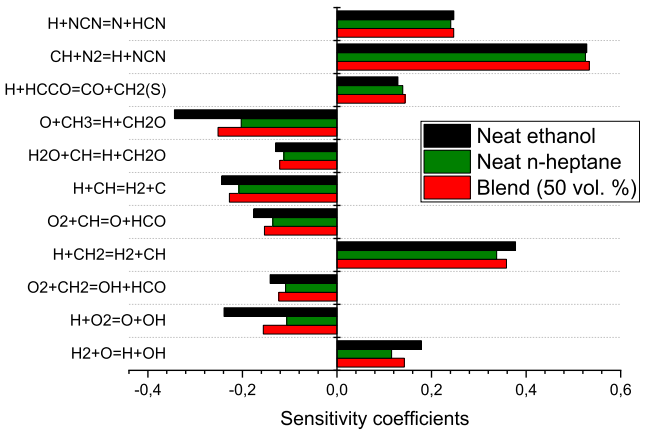

Fig. 6. Normalized NO sensitivity coefficients calculated at $\Phi = 1.4$, HAB = 10 mm, $T_g = 338$ K and $P = 1$ atm for ethanol/air mixtures (black bars), ethanol-n-heptane (50 vol%)/air mixtures (red bars) and n-heptane/air mixtures (green bars). (For interpretation of the references to colour in this figure legend, the reader is referred to the web version of this article.)

thermal-NO formation mainly involve the accuracy of the rate constant for the rate-limiting step (R1), which is on the order of 25% at high temperatures [80]. This uncertainty causes increasing differences when moving from ethanol to n-heptane due to increasing flame temperature. Indeed, in Fig. 5 it can be observed that the sensitivity coefficient for reaction R1 is the highest for n-heptane. In this regard, in our previous work [82], an even higher discrepancy between experiments and POLIMI predictions was observed for ethylene flames, which are characterized by very high flame temperatures. It was concluded that it is possible to correct this problem with a simple modification to the present R1 rate constant. To support this hypothesis, additional simulations at $\Phi = 1$ were carried out by replacing the rate constant of R1 with the value adopted in the Glarborg model [80] to estimate the effect on the prediction interval from the uncertainty of R1. After this modification, the predicted peak X_{NO} decreases by 16, 22, and 29 ppm for ethanol, ethanol/n-heptane and n-heptane, respectively.

On the other hand, it can be noticed from Fig. 3 that the predictions of the prompt-NO route result in significant deviation from the experiments. In particular, in the rich flames, the predicted NO values are as much as 1.6 times higher than the measured values. This is not unexpected considering the lack of experimental data to use as targets on prompt-NO using fuels other than methane, and also considering that prompt-NO is generated from the interaction between fuel and nitrogen chemistry. In detail, the sensitivity analysis with respect to X_{NO} at the conditions of experiments performed at $\Phi = 1.4$, presented in Fig. 6, shows that the amount of NO formed almost exclusively depends on the rate of the prompt mechanism initiation reaction $CH + N_2 = H + NCN$ (R3), which is the most sensitive. Next in importance are reactions that promote/inhibit formation of CH, which are involved in the direct interaction between nitrogen and fuel-oxidation chemistry through reaction (R3). Then, NCN is quickly converted to NO inside the flame zone through a complex sequence of major reactions that involve the interconversion between several fixed nitrogen intermediates such as HCN, HNC, CN, HNCO, H_2CN, HCNH, NCO, HNO, N, NH, NH_2 [80]. Therefore, prediction of the prompt-NO formation requires an accurate rate constant for reaction (R3), as well as the ability to predict CH concentration and the subsequent NCN oxidation. In this regard, the same discrepancies were found in the previous validations of the POLIMI model for ethylene flames [82]. In [82], it was shown that the POLIMI model generally provides a satisfactory prediction of CH profiles, but overestimates the hydrogen cyanide (HCN) concentration in rich flames, which leads to an overestimation of the prompt-NO formation. It was concluded that the description of the balance between HCN formation and consumption, despite that it has been extensively studied over the years, still needs further investigations.

From the data reported in Fig. 3, it can be observed that the amount of NO in ethanol flames, compared to n-heptane and the blend is also lower under rich conditions. As already mentioned above, under fuel rich conditions, NO formation rates do not strongly depend on temperature (see Fig. 4) and the key role is played by the fuel structure. As a matter of fact, the initiation reaction (R3) depends on the formation of CH radicals, which in turn is strongly linked to the fuel-breakdown pathways. In particular, the formation of CH radicals depends on the competition between CH_3 pyrolysis and oxidation routes. In general, under high temperature and rich conditions, the reactions of CH_3 leading to CH radicals are promoted compared to the oxidation pathways leading to acetaldehyde and formaldehyde. Despite the observed discrepancies between experimental and numerical results under fuel rich conditions, the detailed kinetic model is still able to reproduce the lower production of NO in ethanol flames compared to n-heptane flames observed experimentally. Thus, the simulations can be used to elucidate the chemical reactions responsible for the observed behavior. From the numerical analysis, it can be concluded that the presence of an oxygen atom in the ethanol molecule, together with a lower flame temperature compared to n-heptane, stress the CH_3 decomposition/oxidation competition, leading to a slight inhibition of the formation of CH radicals and thus of NO, as shown in Figs. 6 and 7.

Another observation from the data reported in Fig. 3 is that the differences among prompt-NO produced from the three fuels decrease with increasing Φ. For example, in the case of n-heptane, X_{NO} is 42% higher compared to ethanol at $\Phi = 1.2$ and this percentage decreases to 29% at $\Phi = 1.5$, while for the ethanol/n-heptane blend such difference decreases from 25% to 20% in the same equivalence ratio range. While the reproduction of the experimental data is not achieved with the POLIMI model, it is interesting to note that such a decrease of the difference among the three fuels is matched well in relative terms. To explore the chemical nature of this behavior, a sensitivity, rate of production and reaction path analysis was performed. A simple way to summarize the results is to analyze the peak concentration of HCN, which is the predominant cyanide species contributing to the prompt-NO formation in rich flames for the three cases.

The calculated peak mole fraction of HCN is shown in Fig. 8 as a function of Φ for the three investigated fuels. It should be recalled that the kinetic model overpredicts the peak mole fraction of HCN, but the important consideration that provides useful insights here is the qualitative trend and the relative contributions when comparing the three different fuels. Fig. 8 shows that, for the three fuels, the peak mole

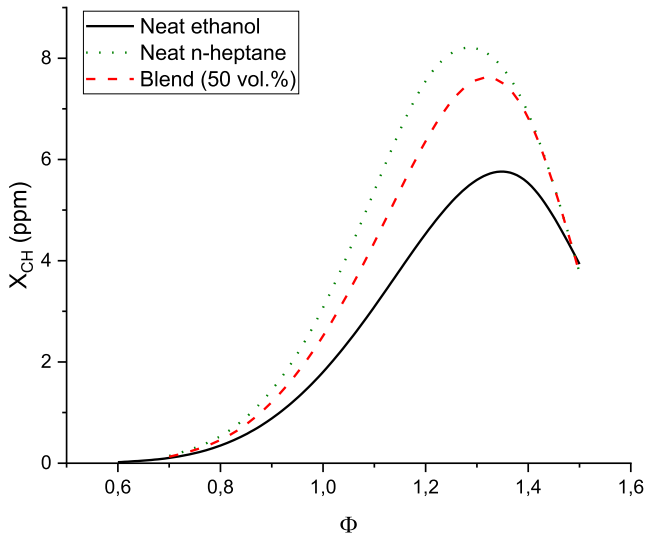

Fig. 7. Calculated peak X_{CH} versus Φ at $T_g = 338$ K and $P = 1$ atm. Black solid line: Ethanol/air mixtures. Red dashed line: ethanol-n-heptane (50 vol%)/air mixtures. Green dotted line: n-heptane/air mixtures.

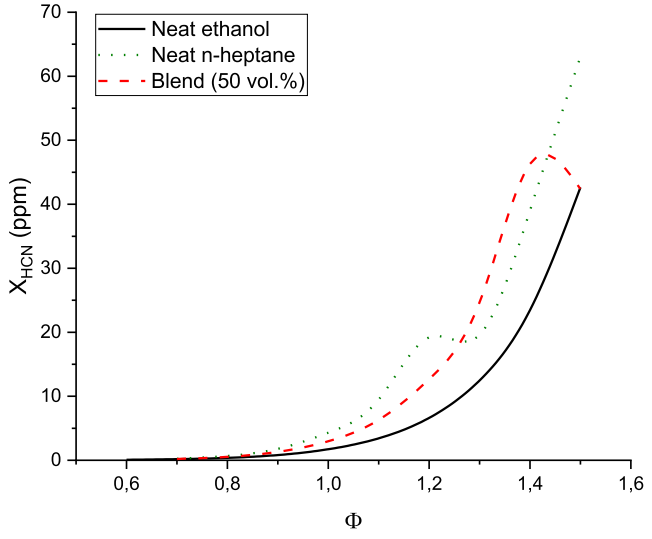

Fig. 8. Calculated peak X_{HCN} versus Φ at $T_g = 338$ K and $P = 1$ atm. Black solid line: Ethanol/air mixtures. Red dashed line: ethanol-n-heptane (50 vol%)/air mixtures. Green dotted line: n-heptane/air mixtures.

fraction of HCN first increases with Φ and it is clearly lower in the ethanol flames compared with the corresponding n-heptane flames due to a lower concentration of hydrocarbon radicals.

Then, for n-heptane, at $\Phi > 1.2$ the peak mole fraction of HCN exhibits an inflection point and then increases rapidly with increasing Φ. A maximum point occurs at $\Phi = 1.4$ in the case of the n-heptane/ethanol blend, while a monotonic trend is visible for ethanol flames in the investigated equivalence ratio range. By comparing Figs. 3 and 8, it is possible to observe that when the peak HCN mole fraction shows a fast increase after the inflection point, the NO mole fraction decreases. Such an inflection point represents a shift in fixed nitrogen partition from NO to HCN, which is caused by a combination of factors. In particular, in the prompt-NO mechanism, the major consumption steps for HCN are represented by the reactions of HCN with O, H, OH, or HCN isomerization. The species formed from these reactions, i.e. NCO, NH, HNC and CN, are rapidly fed into the amine pool, eventually forming NO. However, with increasing Φ, the O-atoms become scarce, inhibiting the conversion of HCN to NO and promoting the reburning mechanism [80]. Reactions between small hydrocarbon radicals (CH, $^3CH_2$, C, HCO, HCCO) and NO then efficiently recycle NO back to HCN. Therefore, the concentration of O-atoms strongly influences the partition between these competing reaction channels. The availability of O-atoms in ethanol-containing flames inhibits the rates of NO consumption through the reburning mechanism, which partially offsets the lower rates of prompt-NO formation. For the same reason, the presence of ethanol in the blend tends to shift the characteristic behavior observed for the neat n-heptane to higher Φ.

In summary, it can be inferred that, for comparable experimental conditions, ethanol, or ethanol containing fuels, produce lower thermal- and prompt-NO emissions than n-heptane. Nevertheless, the difference strongly depends both on the flame stoichiometry and on the amount of ethanol added to n-heptane, thus on the degree of oxygenation. Therefore, ethanol fueling in engines should be tuned and optimized to take into account these effects. In this regard, these results can assist the development of multi-zone engine combustion models. In addition, the present results indicate that, while the available thermochemical models are able to capture the general trends, further adjustments are needed to improve the quantitative capabilities in the predictions of NO formation for variable fuel structures. The information presented above provides valuable data for this important effort. Certainly, more validation experiments and theoretical work are needed to improve these models in order to use them as future design tools. This is particularly true at elevated pressure conditions relevant to engine applications, where additional NO formation pathways may be favored.

4. Conclusion

In this study, an experimental and numerical investigation has been conducted to analyze adiabatic laminar burning velocities and post-flame NO mole fractions in laminar premixed flames burning n-heptane, ethanol and a mixture of them. These flames were experimentally investigated using the heat flux method and LIF over equivalence ratios ranging from 0.6 to 1.5, at atmospheric pressure and initial temperature of 338 K.

The main objectives of this study were to 1) provide advances in fundamental understanding and characterize the effects of the chemical structure of very different fuel molecules on laminar burning velocities and NO formation trends over a broad range of equivalence ratios and 2) supply quantitative data under well-defined ideal conditions that can be used as targets for the development, validation and optimization of detailed kinetic models.

1) It was revealed that with the use of the neat ethanol against neat n-heptane, the laminar burning velocity is increased, and S_L of the ethanol/n-heptane blend is not a weighted average of those associated with the neat constituents.

The analysis of the NO results revealed some interesting features, which shed light on the relevant mechanisms when using fuels with widely different physical and chemical properties. In particular, these measurements confirm that ethanol reduces NO production compared to alkane fuels (n-heptane in this case) at equivalent experimental conditions, in terms of initial temperature, pressure and equivalence ratio. This behavior is due to the slightly lower flame temperatures of ethanol, which decreases the production of thermal-NO at $0.6 < \Phi < 1.2$. While under rich conditions this behavior is due to the tendency of ethanol to produce lower concentrations of CH radicals, thus decreasing the production of prompt-NO, because of the availability of oxygen atoms that promotes the oxidation of methyl groups, inhibiting their decomposition. Under very rich conditions ($\Phi > 1.3$), the lower NO formation through the prompt mechanism in the ethanol flames is partially offset by a lower rate of NO consumption through the reburning mechanism. The importance of these reaction paths increases with increasing initial concentration of ethanol.

2) The measurements have also been compared with simulations

performed using a contemporary comprehensive reaction mechanism available in the literature (POLIMI) that includes detailed chemistry for primary reference fuel and alcohol oxidation, with the addition of NO_x formation. An excellent agreement between the present measurements and simulated results was observed regarding laminar burning velocities over the equivalence ratio range investigated, but discrepancies were observed regarding NO mole fractions, especially under rich conditions. Numerical analyses helped in identifying the main causes of the observed differences. They were mainly attributed to the remaining uncertainty in the rate constant of the thermal-NO initiation reaction under stoichiometric conditions and in the variation of the relative importance of reactions involving hydrogen cyanide consumption pathways under rich conditions. Further improvements can be made by re-evaluation of these reactions to accurately predict NO formation. In this regard, the current measurements provide additional benchmark data of high fidelity, essential for validation and further development of detailed kinetic models.

Funding

This work was supported by the Swedish Energy Agency via the Centre for Combustion Science and Technology [Project KC-CECOST 22538-4], Sweden; the European Research Council [TUCLA 669466]; and the German Research Foundation (DFG) with the research fellowship [ME 5110/1-1, 397116102].

CRediT authorship contribution statement

Marco Lubrano Lavadera: Conceptualization, Data curation, Formal analysis, Investigation, Software, Validation, Visualization, Writing - original draft. **Christian Brackmann:** Conceptualization, Investigation, Methodology, Project administration, Resources, Validation. **Gianluca Capriolo:** Investigation, Validation. **Torsten Methling:** Methodology, Software, Validation. **Alexander A. Konnov:** Conceptualization, Funding acquisition, Project administration, Resources, Supervision.

Declaration of Competing Interest

The authors declare that they have no known competing financial interests or personal relationships that could have appeared to influence the work reported in this paper.

Appendix A. Supplementary data

Supplementary data to this article can be found online at https://doi.org/10.1016/j.fuel.2020.119585.

References

[1] Ajav EA, Singh B, Bhattacharya TK. Experimental study of some performance parameters of a constant speed stationary diesel engine using ethanol-diesel blends as fuel. Biomass Bioenergy 1999;17(4):357–65. https://doi.org/10.1016/S0961-9534(99)00048-3.
[2] Celik MB. Experimental determination of suitable ethanol-gasoline blend rate at high compression ratio for gasoline engine. App Therm Eng 2008;28(5–6):396–404. https://doi.org/10.1016/j.applthermaleng.2007.10.028.
[3] Lapuerta M, Armas O, Herreros JM. Emissions from a diesel-bioethanol blend in an automotive diesel engine. Fuel 2008;87(1):25–31. https://doi.org/10.1016/j.fuel.2007.04.007.
[4] Rakopoulos CD, Antonopoulos KA, Rakopoulos DC. Experimental heat release analysis and emissions of a HSDI diesel engine fueled with ethanol-diesel fuel blends. Energy 2007;32(10):1791–808. https://doi.org/10.1016/j.energy.2007.03.005.
[5] Koç M, Sekmen Y, Topgül T, Yücesu HS. The effects of ethanol-unleaded gasoline blends on engine performance and exhaust emissions in a spark-ignition engine. Renewable Energy 2009;34(10):2101–6. https://doi.org/10.1016/j.renene.2009.01.018.
[6] Costa RC, Sodré JR. Hydrous ethanol vs. gasoline-ethanol blend: Engine performance and emissions. Fuel 2010;89(2):287–93. https://doi.org/10.1016/j.fuel.2009.06.017.
[7] Bielaczyc P, Szczotka A, Woodburn J. The effect of various petrol-ethanol blends on exhaust emissions and fuel consumption of an unmodified light-duty SI vehicle. SAE Technical Paper 2011:24–0177. https://doi.org/10.4271/2011-24-0177.
[8] Wu X, Daniel R, Tian G, Xu H, Huang Z, Richardson D. Dual-injection: the flexible, bi-fuel concept for spark-ignition engines fuelled with various gasoline and biofuel blends. Appl Energy 2011;88(7):2305–14. https://doi.org/10.1016/j.apenergy.2011.01.025.
[9] Masum BM, Masjuki HH, Kalam MA, Rizwanul Fattah IM, Palash SM, Abedin MJ. Effect of ethanol-gasoline blend on NOx emission in SI engine. Renewable Sustainable Energy Rev 2013;24:209–22. https://doi.org/10.1016/j.rser.2013.03.046.
[10] Kumar S, Cho JH, Park J, Moon I. Advances in diesel-alcohol blends and their effects on the performance and emissions of diesel engines. Renewable Sustainable Energy Rev 2013;22:46–72. https://doi.org/10.1016/j.rser.2013.01.017.
[11] Tutak W, Lukács K, Szwaja S, Bereczky Á. Alcohol-diesel fuel combustion in the compression ignition engine. Fuel 2015;154:196–206. https://doi.org/10.1016/j.fuel.2015.03.071.
[12] He BQ, Wang JX, Hao JM, Yan XG, Xiao JH. A study on emission characteristics of an EFI engine with ethanol blended gasoline fuels. Atmos Environ 2003;37(7):949–57. https://doi.org/10.1016/S1352-2310(02)00973-1.
[13] Al-Farayedhi A, Al-Dawood A, Gandhidasan P. Effects of blending crude ethanol with unleaded gasoline on exhaust emissions of SI engine. SAE Technical Paper 2000;2000-01-2857. https://doi.org/10.4271/2000-01-2857.
[14] Hsieh WD, Chen RH, Wu TL, Lin TH. Engine performance and pollutant emission of an SI engine using ethanol-gasoline blended fuels. Atmos Environ 2002;36(3):403–10. https://doi.org/10.1016/S1352-2310(01)00508-8.
[15] Li L, Liu Z, Wang H, Deng B, Xiao Z, Wang Z, Gong C, Su Y. Combustion and emissions of ethanol fuel (E100) in a small SI engine. SAE Technical Paper 2003;2003-01-3262. https://doi.org/10.4271/2003-01-3262.
[16] Durbin TD, Miller JW, Younglove T, Huai T, Cocker K. Effects of fuel ethanol content and volatility on regulated and unregulated exhaust emissions for the latest technology gasoline vehicles. Environ Sci Technol 2007;41(11):4059–64. https://doi.org/10.1021/es061776o.
[17] Najafi G, Ghobadian B, Tavakoli T, Buttsworth DR, Yusaf TF, Faizollahnejad M. Performance and exhaust emissions of a gasoline engine with ethanol blended gasoline fuels using artificial neural network. Appl Energy 2009;86(5):630–9. https://doi.org/10.1016/j.apenergy.2008.09.017.
[18] Zhai H, Frey HC, Rouphail NM, Gonçalves GA, Farias TL. Comparison of flexible fuel vehicle and life-cycle fuel consumption and emissions of selected pollutants and greenhouse gases for ethanol 85 versus gasoline. J Air Waste Manage Assoc 2009;59(8):912–24. https://doi.org/10.3155/1047-3289.59.8.912.
[19] Schifter I, Diaz L, Rodriguez R, Gómez JP, Gonzalez U. Combustion and emissions behavior for ethanol-gasoline blends in a single cylinder engine. Fuel 2011;90(12):3586–92. https://doi.org/10.1016/j.fuel.2011.01.034.
[20] Keskin A, Gürü M. The effects of ethanol and propanol additions into unleaded gasoline on exhaust and noise emissions of a spark ignition engine. Energy Sources Part A 2011;33(23):2194–205. https://doi.org/10.1080/15567030903530558.
[21] Stump FD, Knapp KT, Ray WD. Influence of ethanol-blended fuels on the emissions from three pre-1985 light-duty passenger vehicles. J Air Waste Manage Assoc 1996;46(12):1149–61. https://doi.org/10.1080/10473289.1996.10467550.
[22] Yang HH, Liu TC, Chang CF, Lee E. Effects of ethanol-blended gasoline on emissions of regulated air pollutants and carbonyls from motorcycles. Appl Energy 2012;89(1):281–6. https://doi.org/10.1016/j.apenergy.2011.07.035.
[23] Al-Baghdadi MARS. Measurement and prediction study of the effect of ethanol blending on the performance and pollutants emission of a four-stroke spark ignition engine. Proc Inst Mec Eng 2008;222(5):859–73. https://doi.org/10.1243/09544070JAUTO732.
[24] Yao YC, Tsai JH, Chiang HL. Effects of ethanol-blended gasoline on air pollutant emissions from motorcycle. Sci Total Environ 2009;407(19):5257–62. https://doi.org/10.1016/j.scitotenv.2009.06.017.
[25] Oh H, Bae C, Min K. Spray and combustion characteristics of ethanol blended gasoline in a spray guided DISI engine under lean stratified operation. SAE Int J Engines 2010;3(2):213–22. https://www.jstor.org/stable/26275557.
[26] Lin WY, Chang YY, Hsieh YR. Effect of ethanol-gasoline blends on small engine generator energy efficiency and exhaust emission. J Air Waste Manage Assoc 2010;60(2):142–8. https://doi.org/10.3155/1047-3289.60.2.142.
[27] Chen RH, Chiang LB, Wu MH, Lin TH. Gasoline displacement and NOx reduction in an SI engine by aqueous alcohol injection. Fuel 2010;89(3):604–10. https://doi.org/10.1016/j.fuel.2009.07.015.
[28] Turner D, Xu H, Cracknell RF, Natarajan V, Chen X. Combustion performance of bio-ethanol at various blend ratios in a gasoline direct injection engine. Fuel 2011;90(5):1999–2006. https://doi.org/10.1016/j.fuel.2010.12.025.
[29] Tavares JR, Sthel MS, Campos LS, Rocha MV, Lima GR, da Silva MG, et al. Evaluation of pollutant gases emitted by ethanol and gasoline powered vehicles. Procedia Environ Sci 2011;4:51–60. https://doi.org/10.1016/j.proenv.2011.03.007.
[30] Gravalos I, Moshou D, Gialamas T, Xyradakis P, Kateris D, Tsiropoulos Z. Performance and emission characteristics of spark ignition engine fuelled with ethanol and methanol gasoline blended fuels. In: Manzanera M, editor. Alternative Fuel, InTech; 2011, p.155–174.
[31] Canakci M, Ozsezen AM, Alptekin E, Eyidogan M. Impact of alcohol-gasoline fuel blends on the exhaust emission of an SI engine. Renewable Energy 2013;52:111–7. https://doi.org/10.1016/j.renene.2012.09.062.
[32] Balki MK, Sayin C, Canakci M. The effect of different alcohol fuels on the performance, emission and combustion characteristics of a gasoline engine. Fuel 2014;115:901–6. https://doi.org/10.1016/j.fuel.2012.09.020.

[33] Pang X, Mu Y, Yuan J, He H. Carbonyls emission from ethanol-blended gasoline and biodiesel-ethanol-diesel used in engines. Atmos Environ 2008;42(6):1349–58. https://doi.org/10.1016/j.atmosenv.2007.10.075.

[34] Knoll K, West B, Huff S, Thomas J, Orban J, Cooper C. Effects of mid-level ethanol blends on conventional vehicle emissions. SAE Technical Paper 2009. https://doi.org/10.4271/2009-01-2723. 2009-01-2723.

[35] Hilton B, Duddy B. The effect of E20 ethanol fuel on vehicle emissions. Proc Inst Mec Eng 2009;233(12):1577–86. https://doi.org/10.1243/09544070JAUTO1188.

[36] Cordeiro de Melo TC, Machado GB, de Oliveira EJ, Belchior CRP, Colaço MJ, Barros JEM. Experimental investigation of different hydrous ethanol-gasoline blends on a flex-fuel engine. SAE Technical Paper 2010;2010-36-0469. https://doi.org/10.4271/2010-36-0469.

[37] Gomes P, Ecker R, Kulzer A, Kufferath A, Conti E. Study on boosted direct injection SI combustion with ethanol blends and the influence on the ignition system. SAE Technical Paper 2011;2011-36-0196. https://doi.org/10.4271/2011-36-0196.

[38] Cordeiro de Melo TC, Machado GB, Belchior CRP, Colaço MJ, Barros JEM, de Oliveira EJ, et al. Hydrous ethanol-gasoline blends-combustion and emission investigations on a flex-fuel engine. Fuel 2012;97:796–804. https://doi.org/10.1016/j.fuel.2012.03.018.

[39] Zhuang Y, Hong G. Primary investigation to leveraging effect of using ethanol fuel on reducing gasoline fuel consumption. Fuel 2013;105:425–31. https://doi.org/10.1016/j.fuel.2012.09.013.

[40] Can Ö, Çelikten I, Usta N. Effects of ethanol addition on performance and emissions of a turbocharged indirect injection Diesel engine running at different injection pressures. Energy Convers Manage 2004;45(15–16):2429–40. https://doi.org/10.1016/j.enconman.2003.11.024.

[41] Song CL, Zhou YC, Huang RJ, Wang YQ, Huang QF, Lü G, et al. Influence of ethanol-diesel blended fuels on diesel exhaust emissions and mutagenic and genotoxic activities of particulate extracts. J Hazard Mater 2007;149(2):355–63. https://doi.org/10.1016/j.jhazmat.2007.03.088.

[42] Rakopoulos DC, Rakopoulos CD, Kakaras EC, Giakoumis EG. Effects of ethanol-diesel fuel blends on the performance and exhaust emissions of heavy duty DI diesel engine. Energy Convers Manage 2008;49(11):3155–62. https://doi.org/10.1016/j.enconman.2008.05.023.

[43] Sayin C, Canakci M. Effects of injection timing on the engine performance and exhaust emissions of a dual-fuel diesel engine. Energy Convers Manage 2009;50(1):203–13. https://doi.org/10.1016/j.enconman.2008.06.007.

[44] Huang J, Wang Y, Li S, Roskilly A, Yu H, Li H. Experimental investigation on the performance and emissions of a diesel engine fuelled with ethanol-diesel blends. Appl Therm Eng 2009;29(11–12):2484–90. https://doi.org/10.1016/j.applthermaleng.2008.12.016.

[45] Sayin C. Engine performance and exhaust gas emissions of methanol and ethanol-diesel blends. Fuel 2010;89(11):3410–5. https://doi.org/10.1016/j.fuel.2010.02.017.

[46] Gonca G. Investigation of the effects of steam injection on performance and NO emissions of a diesel engine running with ethanol-diesel blend. Energy Convers Manage 2014;77:450–7. https://doi.org/10.1016/j.enconman.2013.09.031.

[47] Jamrozik A. The effect of the alcohol content in the fuel mixture on the performance and emissions of a direct injection diesel engine fueled with diesel-methanol and diesel-ethanol blends. Energy Convers Manage 2017;148:461–76. https://doi.org/10.1016/j.enconman.2017.06.030.

[48] Emiroğlu AO, Şen M. Combustion, performance and emission characteristics of various alcohol blends in a single cylinder diesel engine. Fuel 2018;212:34–40. https://doi.org/10.1016/j.fuel.2017.10.016.

[49] Karavalakis G, Durbin TD, Shrivastava M, Zheng Z, Villela M, Jung H. Impacts of ethanol fuel level on emissions of regulated and unregulated pollutants from a fleet of gasoline light-duty vehicles. Fuel 2012;93:549–58. https://doi.org/10.1016/j.fuel.2011.09.021.

[50] Zervas E, Montagne X, Lahaye J. Emissions of regulated pollutants from a spark ignition engine. Influence of fuel and air/fuel equivalence ratio. Environ Sci Technol 2003;37(14):3232–8. https://doi.org/10.1021/es026321n.

[51] Marques CST, Barreta LG, Sbampato ME, dos Santos AM. Laser-saturated fluorescence of nitric oxide and chemiluminescence measurements in premixed ethanol flames. Exp Therm Fluid Sci 2010;34(8):1142–50. https://doi.org/10.1016/j.expthermflusci.2010.04.003.

[52] Watson GMG, Versailles P, Bergthorson JM. NO formation in premixed flames of C_1–C_3 alkanes and alcohols. Combust Flame 2016;169:242–60. https://doi.org/10.1016/j.combustflame.2016.04.015.

[53] Watson GMG, Versailles P, Bergthorson JM. NO formation in rich premixed flames of C_1–C_4 alkanes and alcohols. Proc Combust Inst 2017;36(1):627–35. https://doi.org/10.1016/j.proci.2016.06.108.

[54] Bohon MD, Guiberti TF, Sarathy SM, Roberts WL. Variations in non-thermal NO formation pathways in alcohol flames. Proc Combust Inst 2017;36(3):3995–4002. https://doi.org/10.1016/j.proci.2016.05.024.

[55] Bohon MD, Guiberti TF, Roberts WL. PLIF measurements of non-thermal NO concentrations in alcohol and alkane premixed flames. Combust Flame 2018;194:363–75. https://doi.org/10.1016/j.combustflame.2018.05.024.

[56] Brackmann C, Methling T, Lubrano Lavadera M, Capriolo G, Konnov AA. Experimental and modeling study of nitric oxide formation in premixed methanol + air flames. Combust Flame 2020;213:322–30. https://doi.org/10.1016/j.combustflame.2019.11.043.

[57] Kohse-Höinghaus K, Oßwald P, Cool TA, Kasper T, Hansen N, Qi F, et al. Biofuel combustion chemistry: from ethanol to biodiesel. Angew Chem Int Ed 2010;49(21):3572–97. https://doi.org/10.1002/anie.200905335.

[58] Brugman TM, Klein-Douwel R, Huigen G, van Walwijk E, ter Meulen JJ. Laser-induced-fluorescence imaging of NO in an n-heptane- and diesel-fuel-driven diesel engine. Appl Phys B 1993;57:405–10. https://doi.org/10.1007/BF00357383.

[59] Olsson J, Tunestål P, Haraldsson G, Johansson B. A turbo charged dual fuel HCCI engine. SAE Technical Paper 2001;2001-01-1896. https://doi.org/10.4271/2001-01-1896.

[60] Lü X, Hou Y, Zu L, Huang Z. Experimental study on the auto-ignition and combustion characteristics in the homogeneous charge compression ignition (HCCI) combustion operation with ethanol/n-heptane blend fuels by port injection. Fuel 2006;85(17–18):2622–31. https://doi.org/10.1016/j.fuel.2006.05.003.

[61] Lü X, Ji L, Zu L, Hou Y, Huang C, Huang Z. Experimental study and chemical analysis of n-heptane homogeneous charge compression ignition combustion with port injection of reaction inhibitors. Combust Flame 2007;149(3):261–70. https://doi.org/10.1016/j.combustflame.2007.01.002.

[62] Saisirirat P, Foucher F, Chanchaona S, Mounaïm-Rousselle C. Spectroscopic measurements of low-temperature heat release for homogeneous combustion compression ignition (HCCI) n-heptane/alcohol mixture combustion. Energy Fuels 2010;24(10):5404–9. https://doi.org/10.1021/ef100938u.

[63] Saisirirat P, Togbé C, Chanchaona S, Foucher F, Mounaim-Rousselle C, Dagaut P. Auto-ignition and combustion characteristics in HCCI and JSR using 1-butanol/n-heptane and ethanol/n-heptane blends. Proc Combust Inst 2011;33(2):3007–14. https://doi.org/10.1016/j.proci.2010.07.016.

[64] Vuilleumier D, Kozarac D, Mehl M, Saxena S, Pitz WJ, Dibble RW, et al. Intermediate temperature heat release in an HCCI engine fueled by ethanol/n-heptane mixtures: an experimental and modeling study. Combust Flame 2014;161(3):680–95. https://doi.org/10.1016/j.combustflame.2013.10.008.

[65] Xue H, Aggarwal SK. NO_x emissions in n-heptane/air partially premixed flames. Combust Flame 2003;132(4):723–41. https://doi.org/10.1016/S0010-2180(02)00534-5.

[66] Berta P, Aggarwal SK, Puri IK. An experimental and numerical investigation of n-heptane/air counterflow partially premixed flames and emission of NO_x and PAH species. Combust Flame 2006;145(4):740–64. https://doi.org/10.1016/j.combustflame.2006.02.003.

[67] Haas FM, Chaos M, Dryer FL. Low and intermediate temperature oxidation of ethanol and ethanol-PRF blends: an experimental and modeling study. Combust Flame 2009;156(12):2346–50. https://doi.org/10.1016/j.combustflame.2009.08.012.

[68] Dagaut P, Togbé C. Experimental and modeling study of the kinetics of oxidation of ethanol-n-heptane mixtures in a jet-stirred reactor. Fuel 2010;89(2):280–6. https://doi.org/10.1016/j.fuel.2009.06.035.

[69] van Lipzig JPJ, Nilsson EJK, de Goey LPH, Konnov AA. Laminar burning velocities of n-heptane, iso-octane, ethanol and their binary and tertiary mixtures. Fuel 2011;90(8):2773–81. https://doi.org/10.1016/j.fuel.2011.04.029.

[70] Yang C, Wang W, Li Y, Cheng X. Quantitative study on chemical effects of actual/simulated recirculated exhaust gases on ignition delay times of n-heptane/ethanol fuel blends at elevated temperature. Fuel 2020;263:116327. https://doi.org/10.1016/j.fuel.2019.116327.

[71] de Goey LPH, van Maaren A, Quax RM. Stabilization of adiabatic premixed laminar flames on a flat flame burner. Combust Sci Technol 1993;92(1–3):201–7. https://doi.org/10.1080/00102209308907668.

[72] Alekseev VA, Naucler JD, Christensen M, Nilsson EJK, Volkov EN, de Goey LPH, et al. Experimental uncertainties of the heat flux method for measuring burning velocities. Combust Sci Technol 2016;188(6):853–94. https://doi.org/10.1080/00102202.2015.1125348.

[73] Treszczanowicz AJ, Benson GC. Excess volumes for n-alkanols + n-alkanes I. Binary mixtures of methanol, ethanol, n-propanol, and n-butanol + n-heptane. J Chem Thermodyn 1977;9(12):1189–97. https://doi.org/10.1016/0021-9614(77)90119-7.

[74] Orge B, Iglesias M, Rodríguez A, Canosa JM, Tojo J. Mixing properties of (methanol, ethanol, or 1-propanol) with (n-pentane, n-hexane, n-heptane and n-octane) at 298.15 K. Fluid Phase Equilib 1997;133(1–2):213–27. https://doi.org/10.1016/S0378-3812(97)00031-9.

[75] Luque J, Crosley DR. LIFBASE: Database and spectral simulation (version 1.5), SRI International Report, MP 99-009; 1999.

[76] Settersten TB, Patterson BD, Gray JA. Temperature- and species-dependent quenching of NO $A^2\Sigma^+$ ($v' = 0$) probed by two-photon laser-induced fluorescence using a picosecond laser. J Chem Phys 2006;124:234308. https://doi.org/10.1063/1.2206783.

[77] Nakamura H, Shindo M. Effects of radiation heat loss on laminar premixed ammonia/air flames. Proc Combust Inst 2019;37(2):1741–8. https://doi.org/10.1016/j.proci.2018.06.138.

[78] Konnov AA, Dyakov IV, de Ruyck J. Probe sampling measurements and modeling of nitric oxide formation in methane-air flames. Combust Sci Technol 2001;169(1):127–53. https://doi.org/10.1080/00102200108907843.

[79] Lammers FA, de Goey LPH. The influence of gas radiation on the temperature decrease above a burner with a flat porous inert surface. Combust Flame 2004;136(4):533–47. https://doi.org/10.1016/j.combustflame.2003.12.010.

[80] Glarborg P, Miller JA, Ruscic B, Klippenstein J. Modeling nitrogen chemistry in combustion. Prog Energy Combust Sci 2018;67:31–68. https://doi.org/10.1016/j.pecs.2018.01.002.

[81] Klippenstein SJ, Pfeifle M, Jasper AW, Glarborg P. Theory and modeling of relevance to prompt-NO formation at high pressure. Combust Flame 2018;195:3–17. https://doi.org/10.1016/j.combustflame.2018.04.029.

[82] Lubrano Lavadera M, Brackmann C, Konnov AA. Experimental and modeling study of laminar burning velocities and nitric oxide formation in premixed ethylene/air

flames. Proc. Combust. Inst. In Press. https://doi.org/10.1016/j.proci.2020.06.062.
[83] de Persis S, Pillier L, Idir M, Molet J, Lamoureux N, Desgroux P. NO formation in high pressure premixed flames: Experimental results and validation of a new revised reaction mechanism. Fuel 2020;260(15):116331. https://doi.org/10.1016/j.fuel.2019.116331.
[84] Song Y, Marrodán L, Vin N, Herbinet O, Assaf E, Fittschen C, et al. The sensitizing effects of NO_2 and NO on methane low temperature oxidation in a jet stirred reactor. Proc Combust Inst 2019;37(1):667–75. https://doi.org/10.1016/j.proci.2018.06.115.
[85] Matveev SS, Idrisov DV, Matveev SG, Konnov AA. Laminar burning velocities of surrogate components blended with ethanol. Combust Flame 2019;209:389–93. https://doi.org/10.1016/j.combustflame.2019.08.010.
[86] Sileghem L, Alekseev VA, Vancoillie J, Nilsson EJK, Verhelst S, Konnov AA. Laminar burning velocities of primary reference fuels and simple alcohols. Fuel 2014;115:32–40. https://doi.org/10.1016/j.fuel.2013.07.004.
[87] Sileghem L, Alekseev VA, Vancoillie J, Van Geem KM, Nilsson EJK, Verhelst S, et al. Laminar burning velocity of gasoline and the gasoline surrogate components iso-octane, n-heptane and toluene. Fuel 2013;112:355–65. https://doi.org/10.1016/j.fuel.2013.05.049.
[88] Holley AT, Dong Y, Andac MG, Egolfopoulos FN. Extinction of premixed flames of practical liquid fuels: experiments and simulations. Combust Flame 2006;144(3):448–60. https://doi.org/10.1016/j.combustflame.2005.08.001.
[89] Sarathy SM, Oßwald P, Hansen N, Kohse-Höinghaus K. Alcohol combustion chemistry. Prog Energy Combust Sci 2014;44:40–102. https://doi.org/10.1016/j.pecs.2014.04.003.
[90] Capriolo G, Brackmann C, Lubrano Lavadera M, Methling T, Konnov AA. An experimental and kinetic modelling study on nitric oxide formation in premixed C3 alcohol flames. Proc. Combust. Inst. In Press. https://doi.org/10.1016/j.proci.2020.07.051.